Supporting Information

Efficient Caustic and Hydrogen Production Using a Pressurized Flow-Through Cathode

Fan Yang, Minhao Xiao[b], Sangsuk Lee, Javier Alan Quezada Renteria, Xinyi Wang, Minju Cha , Anya Dickinson-Cove, Sungsoon Kim, Guy Ramon, Gaurav N. Sant , Eric M. V. Hoek ，and David Jassby *

Corresponding Author

***David Jassby**. Tel: (310) 825-1346. E-mail: jassby@ucla.edu

Experimental section

4.1. Materials and chemicals: Carboxyl group functionalized single-walled CNT (SWNT-COOH) with a diameter of 1-4 nm was purchased from Cheap Tubes Inc. (USA). Polysulfone UF membrane (PS-35) was generously provided by Solecta (Oceanside, CA) and used as is. Nickel sulfate heptahydrate ($NiSO_4 \cdot 7H_2O$, 98% Alfa Aesar), nickel chloride hexahydrate ($NiCl_2 \cdot 6H_2O$, reagent grade, Sigma Aldrich), boric acid (H_3BO_3, ACS grade, Fisher-scientific), sodium dodecylbenzene sulfonate (SDS, technical grade, Fisher-scientific), sodium chloride (NaCl, 99%, Fisher-scientific) were used as received.

4.2. Ni/CNT cathode fabrication: The cathode fabrication process, as outlined in previously published works [1], was briefly described as follows: Initially, 0.3 g of SWNT/COOH was dispersed in 1 L of water, with 10 g of SDS added as a surfactant to enhance the stability of the suspension. Subsequently, the suspension underwent sonication using a horn sonicator. at 70% amplitude for 30 minutes, with cycles of 1 second on and 1 second off. The suspension was then centrifuged at 12500 rpm and 4 °C for 15 minutes. The supernatant was collected and subjected to two additional rounds of centrifugation before being used as the final product for CNT coating. Following this, 20 ml of a 0.3 g/L CNT suspension was pressure deposited on a PS30 membrane, and the resulting composite was dried for 30 minutes at 80 °C prior to use. The Ni layer was applied to the CNT coating using the electrodeposition method. To prepare the solution, 25 mM of $NiCl_2 \bullet 6H_2O$, 150 mM of $NiSO_4 \bullet 7H_2O$ were dissolved in water, and the solution was adjusted to pH of 6 prior to use. An external DC power supply (model: KA3005P, KORAD brand, Shenzhen, China) was then employed to establish an electric field between the cathode and a nickel 200 plate (McMaster-Carr,

Atlanta, GA, USA) anode for the electrodeposition of nickel onto the CNT layer. The deposition process operated at a current density of 10 A/m² for 10 minutes.

4.3. *Operation of flow-through cathode system*: The system, as utilized in previously published works [1], comprises a customized cross-flow cathode system that includes a diaphragm pump, pressure relief valve, pulsation dampener, pressure cell, pressure regulator, pressure gauge, balance, and computer. The pressure within the system is regulated by a pressure regulator, and the permeate flux is monitored by a balance that records the weight of the collected permeate, exporting data every 5 seconds. Prior to initiating the experiments, the cathode is compressed at 300 psi for 30 minutes. The power supply is set to constant voltage mode for the duration of the experiments. After running each experiment for 10 minutes, a 5 ml sample is collected, and its pH is measured.

4.4. *SEC calculation*:

The SEC of the process was calculated using:

$$SEC\ (kWh/kg\ NaOH) = \frac{U \cdot I \cdot t}{n \cdot M} = \frac{U \cdot I}{J_W \cdot \rho \cdot A}$$

where U is the cell voltage (in V), I is the current (in A), t is the time period (in hour), M is the molar mass (40 kg/kmol for NaOH), n is the produced molar amount (in mol), Jw is the water flux (in LMH), ρ is the mass concentration of NaOH (in kg/L), and A is the cathode area (in m^2)

4.5. *Current efficiency calculation*:

The current efficiency of the process was calculated using:

$$Current\ Efficiency\ (\%) = \frac{n}{Q/F}$$

where Q is the charge (in C), and F is Faraday's constant (96485 C/mol).

4.6. Hydrogen gas collection and measurement:

Hydrogen gas was collected from the permeate outlet of the system using the displacement method. A voltage of 3 V was applied to a 3.5% Na_2SO_4 feed solution, and the gases in the permeate stream were directed into a container filled with water and inverted in the water bath. The container was equipped with a valve at one end, which was connected to a gas bag. Gas samples were collected using gas-tight syringes to prevent any contamination or loss of volatile components. Each sample was then injected into the heated inlet of a gas chromatograph (7890B, Agilent, United States), equipped with a thermal conductivity detector (TCD), using helium as the carrier and reference gas. The chromatographic separation was performed on a capillary column suitable for gaseous components. The temperature of the column was programmed to optimize the separation of different gas species. The identity and concentration of the components were determined by comparing the retention times and peak areas to those of known standards run under identical conditions.

4.7. *Materials characterization*: The electrical conductivity of the cathode was characterized through measurement of its sheet resistance using a 4-point conductivity meter (MCP-T610, Mitsubishi Chemical Analytech Co., Japan). SEM imaging was performed using a ThermoFisher Phenom Pharos G2 Desktop SEM FEG-SEM, sourced from Nanoscience Instruments (VA, USA). Images were taken for each cathode at magnifications up to 200,000×. For surface imaging, a 50%/50% combination of backscattered electron detector (BSD) and secondary electron detector (SED) were employed, while for cross-sectional imaging, only BSD was utilized. Elemental mapping of surfaces were performed using EDS (Phenom Pharos G2 Desktop FEG-SEM, Thermo Fisher). Spinning-disk confocal microscopy was used to characterize bubble evolution on the cathode surface during water electrolysis. Leica DMI 5000M equipped with a Yokogawa CSU-X1 spinning disk module rotated at 5000rpm was used for imaging, employing a Mitutoyo

10x/0.28NA dry long working distance objective lens. A stage insert was designed and 3D printed in polyethylene terephthalate glycol (PETG) to accommodate the large size of the objective lens, focus on bubbles forming on the cathode surface, and stably secure the experimental apparatus for large area tilescans. Fluorescein was added to the media for confocal fluorescence imaging, illuminated by a HÜBNER Cobolt 06-MLD 488nm CW laser and emissions collected through 525/550 filter. Triggering was synced from a Hamamatsu ORCA-Flash4.0 LT acquiring images of 564 um x 511 um pixel resolution, with z-steps of 300 um. All imaging hardware was controlled by Micro-Manager (v2.0-gamma). The whole map of 15 × 15 sub- images were stitched with ImageJ. The stitched picture with dimension of 8.45 mm × 7.66 mm was further processed using image J plugin: ComDet v0.5.5, where gas bubbles was Hough circle transformed to circles that the machine can distinguish. Then the dimensions and quantities of gas bubbles was summarized through processed images.

4.8. *Electrochemical characterization*: EIS and LSV were conducted in the flow cell with 3.5% NaCl electrolytes, and recorded using an electrochemical workstation (Biologic, SP-50e) with a 3-electrode setup where a Ag/AgCl wire was used as reference electrode. EIS measurements were performed over a range of frequencues (20 mHz to 100 kHz), with bias of -0.90, -1.36, -1.79, -2.22 V vs. Ag/AgCl wire and 300 mV amplitude. EIS curves were fitted using Zview (version 3.1). LSV measurements on the cathode were performed at a scan rate of 5mV/s. The half-cell potential of the cathode was measured vs. a Ag/AgCl wire reference.

4.9. *COMSOL Multiphysics* was utilized to conduct a 2D numerical analysis of a crossflow channel equipped with a cathode and an anode. Two primary variables were examined: (i) variations in water flux due to different applied pressures, with five distinct water flux conditions simulated, and (ii) varying cross-flow velocities within the channel. The Tertiary Current Distribution Module

was used to investigate electrode reactions coupled with hydrodynamic mass transport under steady-state conditions. The dimensions of the channel were set at a height of 2 mm and a length of 30 mm. Spatially averaged values were calculated over a central section of the crossflow channel, 0.5 mm in width, to smooth out local fluctuations and better reflect the interactions between the cathode and anode. The cathode, CNT/Ni layer with a thickness of 0.5 μm, was maintained at a voltage of -1.36 V, while the anode was set at 1.14 V. This setup facilitated the simulation of water splitting, with the anode producing chlorine and protons and the cathode generating hydroxide ions. Equilibrium potentials were calculated using the Nernst equation, and the Butler-Volmer equation was applied to determine the current density at the electrodes. Based on experimental data, the exchange current density was set at 0.044 A/m^2, and a limiting current density of 1500 A/m^2 was chosen, slightly exceeding the experimentally measured value. The electrode's active specific surface area was considered to be 50000 m^{-1}, as indicated in prior studies, with anodic and cathodic transfer coefficients set at 0.5. The porosity and tortuosity of the cathode were assigned values of 0.1 and 7, respectively. A flux boundary was established at the bottom of the cathode to impose water flux in the system.

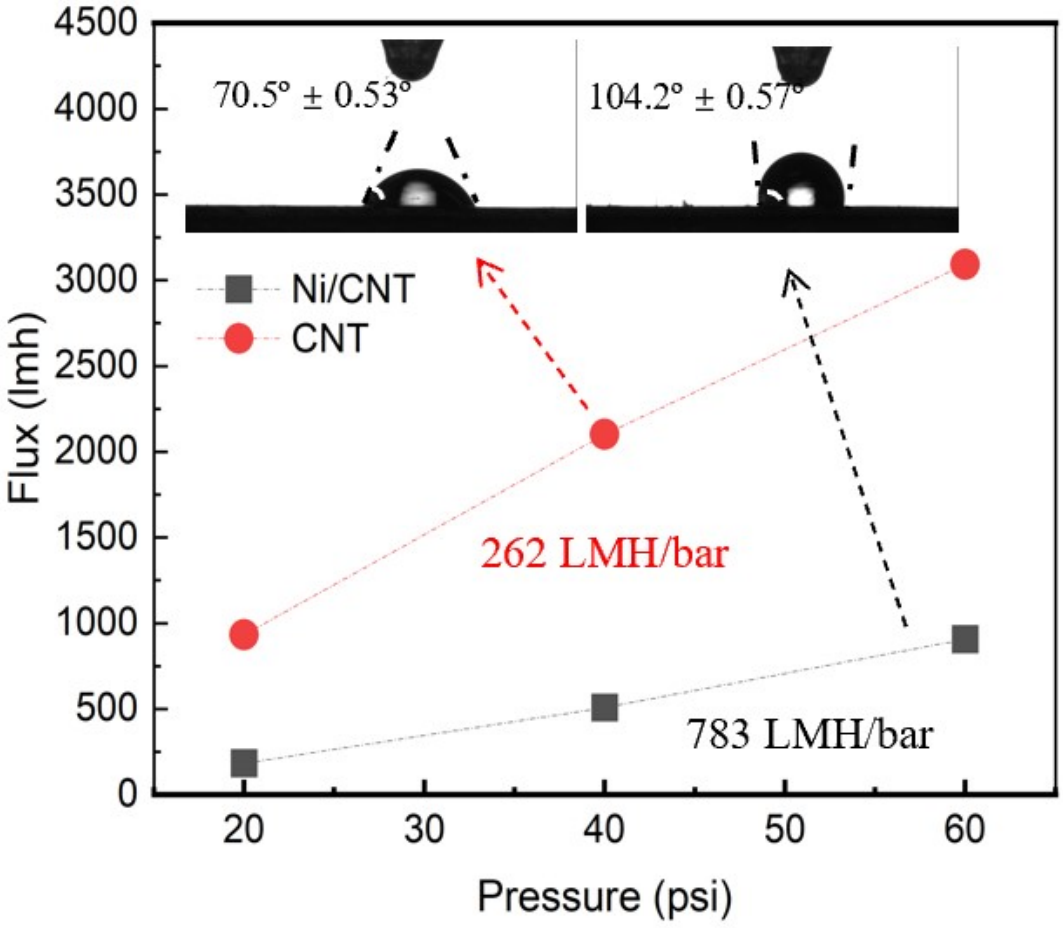

Figure S1. Flux vs. pressure plot of Ni/CNT membrane and CNT membrane, where the red line represents the CNT membrane and the black line represents the Ni/CNT membrane. The tested solution was DI water. The slope of the linear fit indicates membrane permeability: the CNT membrane has a permeability of 783 LMH/bar, while the CNT/Ni membrane has a permeability of 262 LMH/bar. The insets show contact angle measurements of the CNT membrane and the CNT/Ni membrane.

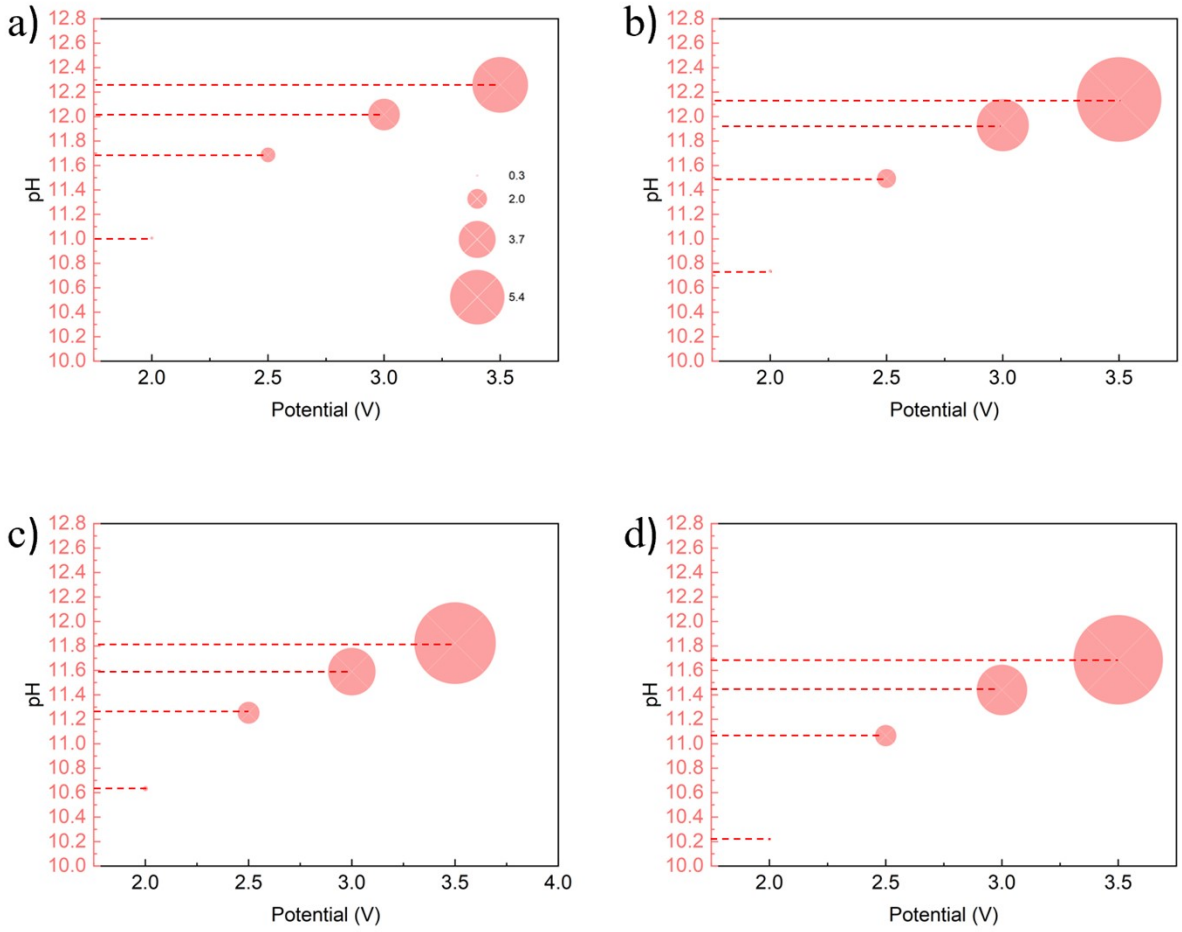

Figure S2. Hydroxide ion flux and pH of permeate vs. potentials, where the y-axis represents pH, and the red circles represent hydroxide ion flux (unit: mol/m²/hr). The size of the circles indicates the magnitude of the flux. The tested solution was 3.5% NaCl. The graphs show data for different permeate flux rates: a) 300 LMH, b) 600 LMH, c) 1200 LMH, d) 1800 LMH.

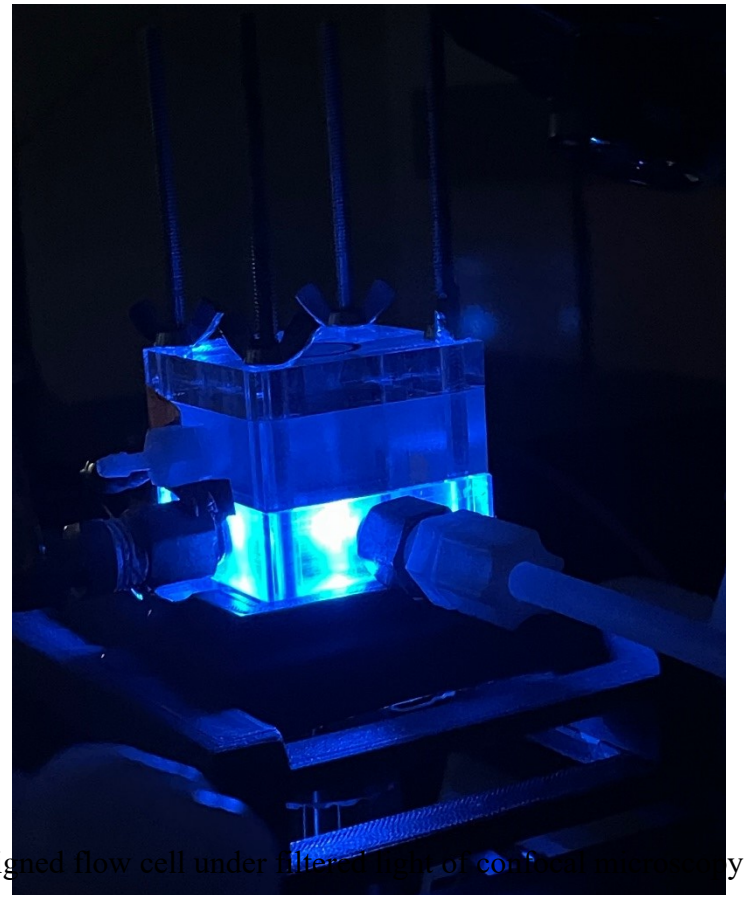

Figure S3. Designed flow cell under filtered light of confocal microscopy for gas bubble characterization.

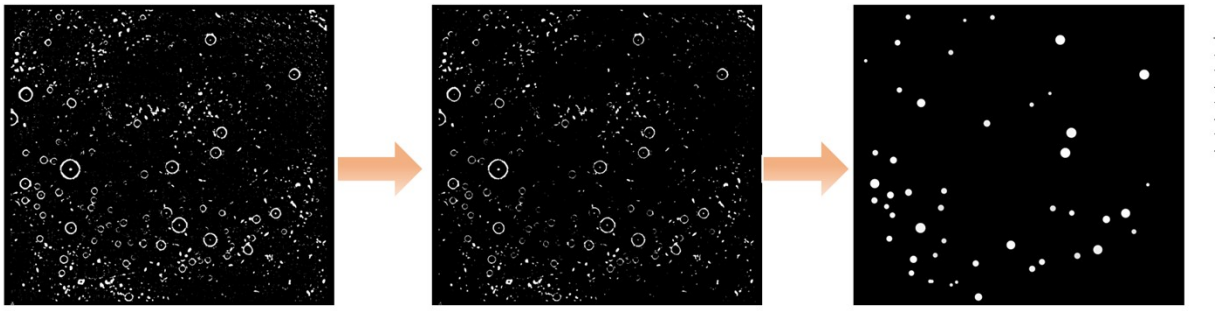

Figure S4. The image processing procedures to transform raw images to images that allow for the quantification of gas bubble numbers and size distribution

Gas bubbles distribution over electrode’s surface

As shown in Fig. S5, the bubble size distribution is quite broad, ranging from 20 μm to 250 μm. When analyzing the images under varying pressure, it is clear that the number of bubbles decreases as the pressure increases. Additionally, when flux > 0 (Fig. S5a), the bubble count decreases more significantly with increasing pressure compared to the conditions without flux (Fig. S5b), indicating that flux also influences bubble formation. In the groups with varying flow rates (Fig. S5c), we observed that the number of bubbles decreases as the flow rate increases. This clearly demonstrates that the bubble count is highly correlated with pressure, flux, and flow rate.

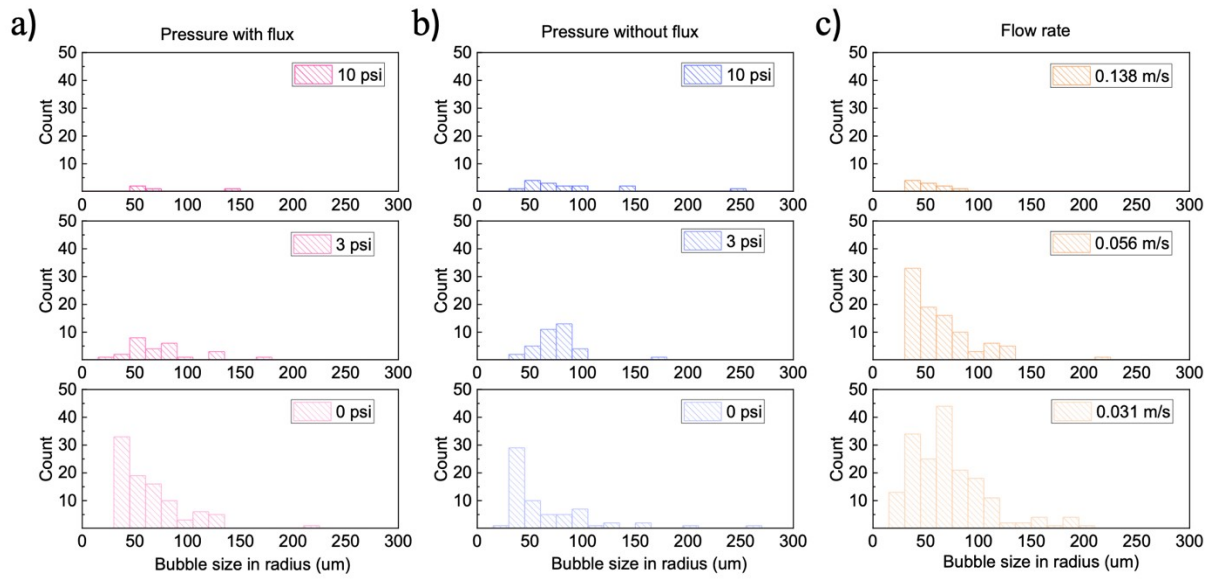

Figure S5. Hydrogen gas bubble size distribution in different conditions: a) different pressures with fluxes (0 psi, 3 psi, 10 psi), where the cross flow velocity was fixed at 0.056 m/s; (b) different pressures without permeate flux (0 LMH at 0 psi, 160 LMH at 3 psi, 540 LMH at 10 psi), where cross flow velocity was fixed at 0.056 m/s; (c) different cross flow velocities (0.031 m/s, 0.056 m/s, 0.138m/s), where the pressure was fixed at 0 psi.

Bubble Effects on Ohmic Overpotential

The gas void fraction significantly affects ohmic losses in electrochemical systems. Bubbles attached to electrode surfaces or dispersed in the electrolyte create additional resistance by reducing the available pathways for ion migration, thereby lowering the effective conductivity of the electrolyte. Empirical models describe the relationship between gas void fraction and the relative conductivity of the electrolyte.[2] According to Maxwell's and Bruggemann's relations, the void fraction (ε) correlates with the relative conductivity of gas dispersions, which has been validated for void fractions relevant to water electrolysis ($\varepsilon = 0-0.12$) [3, 4] :

$$\frac{k}{k_0} = (1-\varepsilon)^{3/2}$$

where k and k_0 are respectively the conductivity of the electrolyte in the presence and absence of bubbles and ε is the gas void fraction.

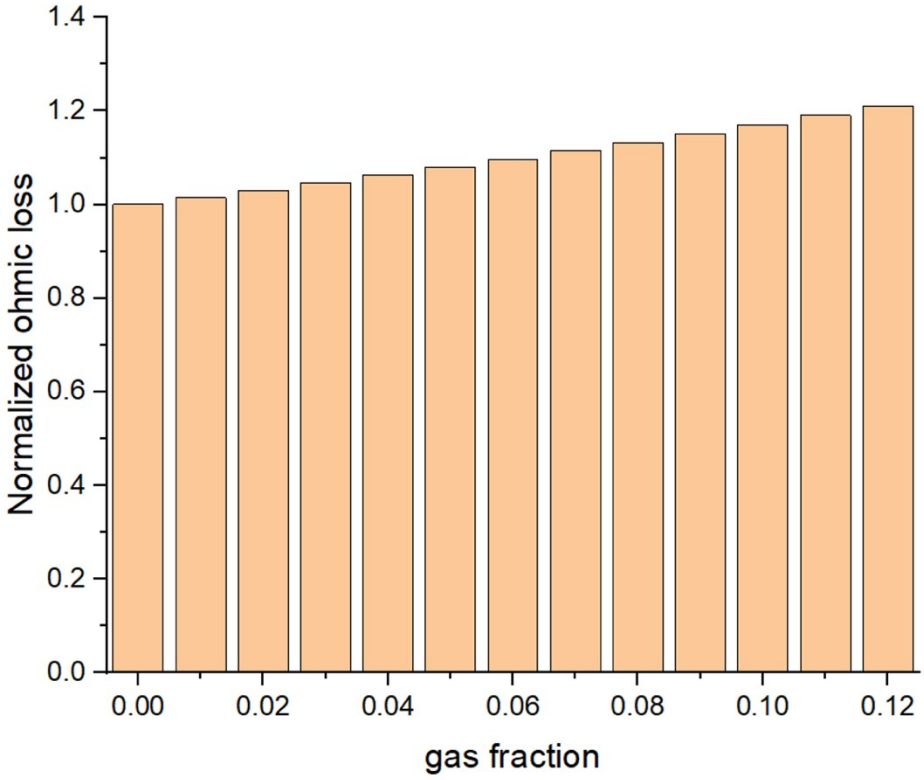

Figure S6. The relationship between normalized ohmic loss and gas fraction void fraction

Bubble Effects on Activation Overpotential

Gas bubble coverage affects activation overpotential by decreasing the effective electrocatalytic surface area, which increases the overpotential (η) for a given current density. The current density (j) is related to the fractional bubble coverage (σ) by the geometric relationship [5]:

$$j = \frac{i}{A(1-\sigma)}$$

Where i is current, and A is area.

At low current densities ($j \rightarrow 0$), kinetic losses dominate over ohmic losses, and the activation overpotential can be described by the bubble coverage fraction (σ) as follows [5]:

$$\eta = \frac{RT}{F} ln \frac{1}{1-\sigma}$$

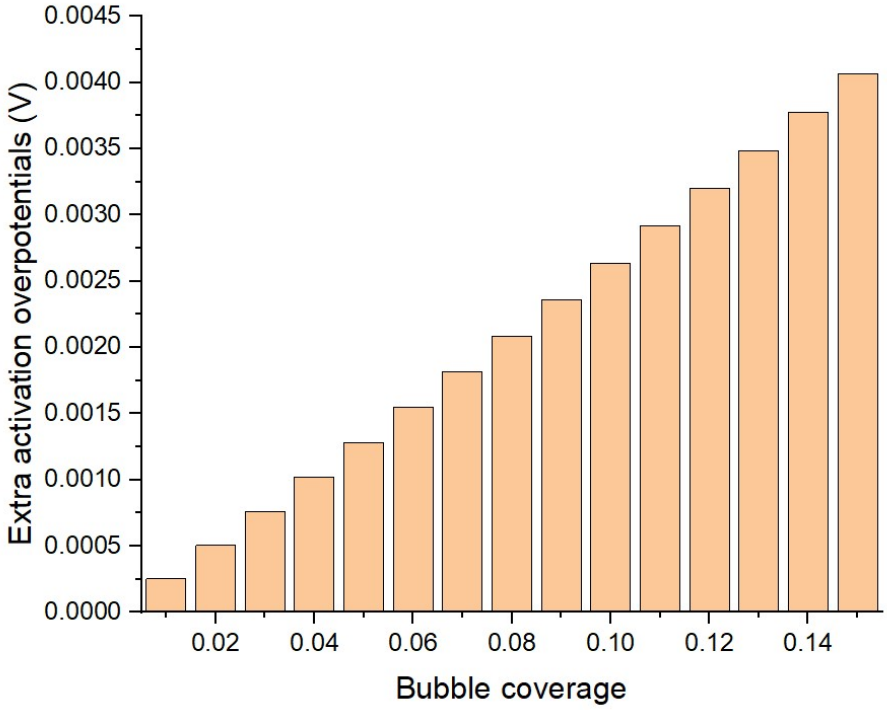

Figure S7. The relationship between extra activation overpotentials and gas bubble coverage

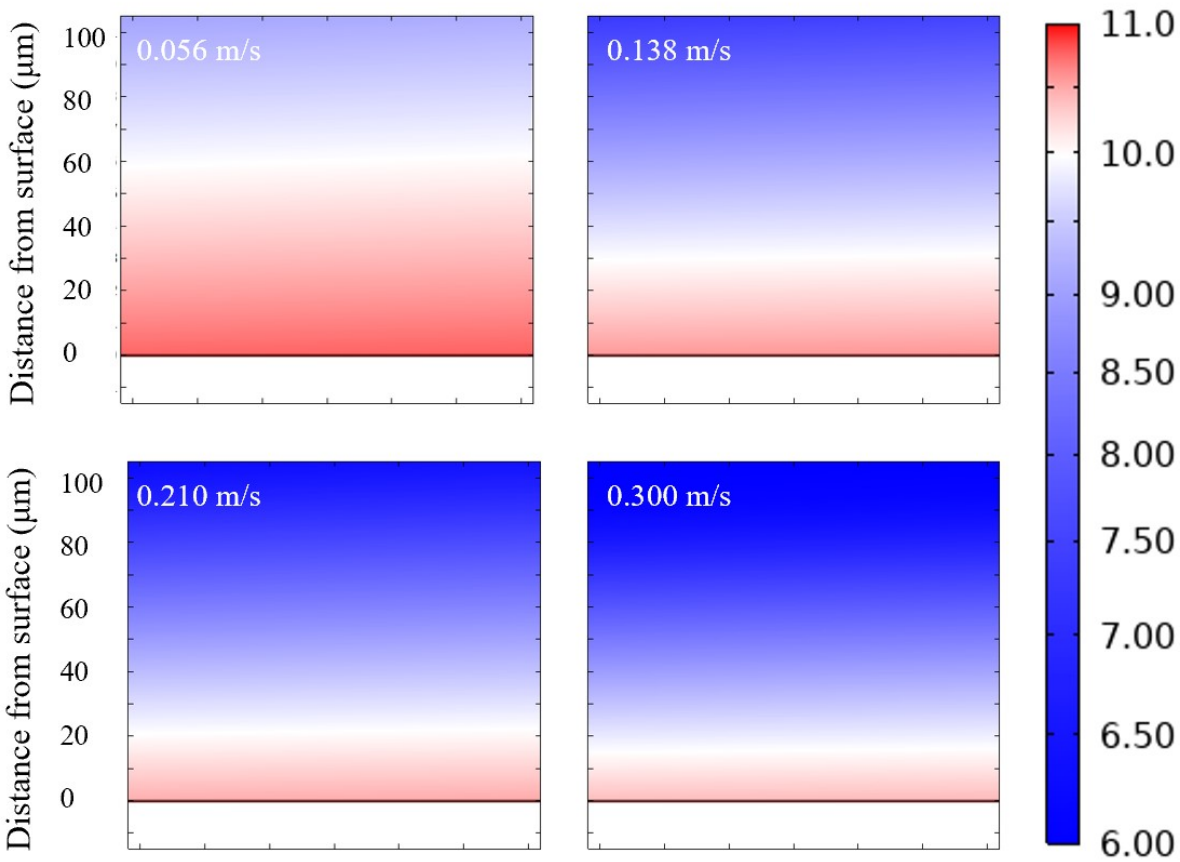

Figure S8. Simulated changes in hydroxide ion concentration near cathode surface at different cross flow rate (0.056 m/s, 0.138 m/s, 0.210m/s, and 0.300 m/s).

Reference:

1. K. Schwabe, M. Nemati, R. Amin, Q. Tran and D. Jassby, *Nature Sustainability*, 2020, 1-8.
2. A. Angulo, P. van der Linde, H. Gardeniers, M. Modestino and D. F. Rivas, *Joule*, 2020, **4**, 555-579.
3. J. C. Maxwell, *A treatise on electricity and magnetism*, Oxford: Clarendon Press, 1873.
4. L. Sigrist, O. Dossenbach and N. Ibl, *Journal of applied electrochemistry*, 1980, **10**, 223-228.

5. J. Dukovic and C. W. Tobias, *Journal of the Electrochemical Society*, 1987, **134**, 331.